Bistability of vortex core dynamics in a single perpendicularly magnetized nano-disk

G. de Loubens, A. Riegler, B. Pigeau, F. Lochner, F. Boust, K.Y. Guslienko, H. Hurdequint, L.W. Molenkamp, G. Schmidt, A. N. Slavin, et al.

Bistability of vortex core dynamics in a single perpendicularly magnetized nano-disk

G. de Loubens,[1,*] A. Riegler,[2] B. Pigeau,[1] F. Lochner,[2] F. Boust,[3] K.Y. Guslienko,[4] H. Hurdequint,[5] L.W. Molenkamp,[2] G. Schmidt,[2] A. N. Slavin,[6] V. S. Tiberkevich,[6] N. Vukadinovic,[7] and O. Klein[1]

[1]*Service de Physique de l'État Condensé (CNRS URA 2464), CEA Saclay, 91191 Gif-sur-Yvette, France*
[2]*Physikalisches Institut (EP3), Universität Würzburg, 97074 Würzburg, Germany*
[3]*ONERA, Chemin de la Hunière, 91761 Palaiseau, France*
[4]*Department of Materials Physics, The University of the Basque Country, 20080 San Sebastian, Spain*
[5]*Laboratoire de Physique des Solides, Université Paris-Sud, 91405 Orsay, France*
[6]*Department of Physics, Oakland University, Michigan 48309, USA*
[7]*Dassault Aviation, 78 quai Marcel Dassault, 92552 Saint-Cloud, France*

(Dated: December 22, 2008)

Microwave spectroscopy of individual vortex-state magnetic nano-disks in a perpendicular bias magnetic field, H, is performed using a magnetic resonance force microscope (MRFM). It reveals the splitting induced by H on the gyrotropic frequency of the vortex related to the existence of the two stable polarities of the core. This bistability extends up to a large negative (antiparallel to the core) value of the bias magnetic field H_r, at which the core polarity is reversed. The difference between the frequencies of the two stable rotational modes of each polarity is proportional to H and to the ratio of the disk thickness to its radius. Simple analytic theory in combination with micromagnetic simulations give quantitative description of the observed bistable dynamics.

Magnetic vortices are singular topological states found in the equilibrium magnetic configuration of sub-micron size ferromagnetic dots [1, 2]. In a certain range of dot aspect ratios (ratio $\beta = t/R$ of the dot thickness t to its radius R) the equilibrium ground state of the static magnetization consists of the curling in-plane magnetization and a nanometer size core of the out-of-plane magnetization at the dot center. The magnetization of the vortex core can point either up or down, both polarities $p = \pm 1$ being degenerate at remanence. This bi-stable property of magnetic vortices, as well as the switching from one polarity to the other, have been intensively studied in the past few years because of their possible applications in magnetic storage devices [3, 4, 5]. It has already been established (i) that the lowest excitation mode of the vortex state is the gyrotropic mode corresponding to a rotation of the vortex core about the dot center and (ii) that the frequency of this mode can be tuned linearly by the dot aspect ratio β [6].

In this Letter, we report on the experimental observation of bistability of the vortex core dynamics in a *single* magnetic disk subjected to the perpendicular bias magnetic field, that is changing from positive (parallel to the vortex core) to negative (antiparallel to the vortex core) values. We demonstrate that in a certain range of the bias field magnitudes there are two stable gyrotropic modes of the vortex core rotation having different frequencies and opposite circular polarizations, and corresponding to opposite orientations of the vortex core relative to the direction of the bias magnetic field. The difference in frequencies of these two stable gyrotropic modes is proportional to the magnitude of the applied bias field, H, and, also, to the dot aspect ratio β. We believe that this easily controlled dynamic bistability might be important for the development of novel magnetic memory elements.

Our experiments were performed by means of a magnetic resonance force microscope (MRFM) [7] on individual nano-disks of thickness $t = 43.8$ nm and two different radii ($R_1 = 130$ and $R_2 = 520$ nm) made of NiMnSb, a soft conductive magnetic material that has very low magnetic losses (typical Gilbert damping constant is $\alpha = 0.002 - 0.003$). The disk samples were placed in the uniform external bias magnetic field oriented perpendicular to the disk plane and having magnitude that was continuously varied from -10 to $+10$ kOe.

The nano-disks were fabricated from an epitaxially grown NiMnSb film deposited on an InP(001) substrate [8]. A reference sample of a continuous film was cut out of the same film for characterization purposes. Disks of different diameters were patterned using electron beam lithography and ion milling techniques. A 50 nm thick Si_3N_4 cap layer was deposited on top of the disks for protection. Subsequently, the microwave antenna, which consists of a 300 nm thick Au layer, was deposited on top of the disks. The antenna consists of an impedance matched strip-line terminated by a micron-size short. The short behaves as an anti-node of magnetic field and it generates a linearly polarized microwave magnetic field oriented in-plane perpendicularly to the stripe direction.

The detection scheme of MRFM [7] is inspired by magnetic force microscopy (MFM). It consists of an ultra-soft cantilever with a 800 nm diameter sphere of amorphous Fe (coercitivity < 10 G) glued to its apex (see Fig.1a). MRFM spectroscopy is achieved by placing the center of the sphere above the center of the nano-disk (cf. image of the $R_1 = 130$ nm disk in Fig.1b) and producing a microwave field excitation with the antenna. The microwave power is switched ON and OFF (source modulation) at the cantilever resonance frequency. A ferromagnetic resonance (FMR) spectrum is obtained by

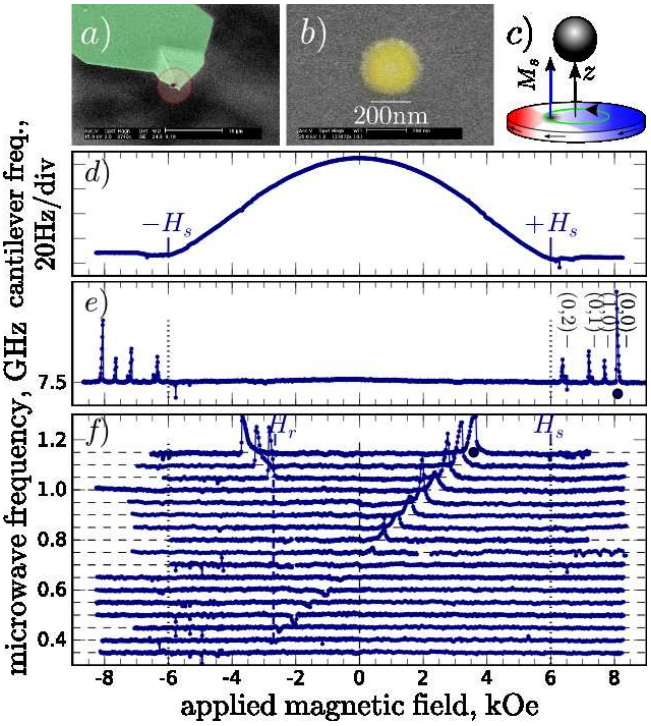

FIG. 1: (Color online) (a) Image of the magnetic probe (Fe sphere glued to the tip of the cantilever); (b) Image of the $R_1 = 130$ nm NiMnSb nano-disk; (c) Detection scheme: the rotating vortex core is sensed through the dipolar force induced on the probe; (d) The cantilever frequency, proportional to M_z, the vertical component of the static magnetization of the nano-disk, as a function of the perpendicular bias magnetic field H; (e) Nano-disk excitation spectrum in the saturated regime ($|H| > H_s$) recorded at 7.5 GHz; (f) Excitation spectra in the vortex (unsaturated) state ($|H| < H_s$).

recording the vibration amplitude of the cantilever as a function of the perpendicular bias magnetic field H at constant microwave excitation frequency. During the scan, the cantilever resonance frequency is also recorded (Fig.1d). This enables static magnetometry of the sample. The saturation field of the $R_1 = 130$ nm nano-disk is $H_s = \pm 6$ kOe, which marks the region of the maximum radial susceptibility.

Fig.1e shows the FMR spectrum of the smaller nano-disk at the frequency of 7.5 GHz. Above the saturation field H_s, the excitation spectrum of the disk consists of a series of peaks corresponding to the confined dipole-exchange spin-wave modes of the disk. Their quantized resonance frequencies (resonance fields) are given by Eq.(1) from [9]. These modes are labeled with a pair (l, m) of azimutal and radial mode indices [7]. The lowest $(0, 0)$ (and the most spatially uniform) spin wave mode of the disk (Kittel mode) is situated at 8.1 kOe and is marked by a blue circle symbol. The frequency of this lowest quasi-uniform mode ω_K can be approximately described as:

$$\omega_K(H) = \gamma\{H - H_K\}, \qquad (1)$$

where $H_K = 4\pi M_s(N_{zz} - N_{rr}) - H_A$. Here M_s is the saturation magnetization, N_{ii} are the diagonal elements of the effective demagnetization tensor of the uniformly magnetized disk. H_A is a uniaxial perpendicular anisotropy field (easy-plane for $H_A < 0$), and γ is the gyromagnetic ratio. All the parameters used in Eq. (1) were measured independently using the reference film sample by means of standard magnetometry and cavity-FMR techniques (results are presented in table I). The calculated position of the Kittel mode (as well as the positions of the higher modes calculated using Eq. (1) from [9]) are shown near the corresponding index pairs in Fig.1e. This calculation did not use any adjustable parameters and took into account the stray field of the cantilever probe (around 500 Oe) [7]. The analytically calculated values of H_K for the smaller and larger disks are $H_K \approx 5.7$ kOe and $H_K \approx 8.0$ kOe, respectively.

TABLE I: Physical parameters of the reference NiMnSb layer.

4πMs (G)	γ (rad.s^{-1}.G^{-1})	H_A (G)	α
6.9×10^3	1.8×10^7	-1.85×10^3	2.3×10^{-3}

When the external bias magnetic field H is reduced below the saturation field H_s, a single magnetic vortex is formed inside the nano-disk (which can be visualized by standard MFM). Fig.1f shows the dynamical behavior of the vortex-state disk (unsaturated regime). The measured mechanical signal originates from the reduction of the dipolar coupling between the disk and the sphere during the microwave excitation sequence (see Fig.1c). It is associated with the lateral displacement of the vortex core position, which moves away from the center of the disk during the gyration motion [4, 10]. Such signal is sensitive to the polarity of the vortex core.

The baseline of each spectrum in Fig.1f is set at the excitation frequency. The spectrum for 1.15 GHz has an intense peak at around +3.5 kOe (blue circle) corresponding to the excitation of the gyrotropic mode of the vortex core, as well as its mirror image at −3.5 kOe. The gyrotropic frequency decreases with the bias magnetic field H, and in the zero field ($H = 0$) has the value of 0.7 GHz. In the region of negative bias fields $H < 0$ the mode continues to exist, but the corresponding resonance peak has a negative amplitude, which indicates that now the direction of the bias field is opposite to that of the vortex core. The gyrotropic frequency continues to decrease with the same slope until the bias field value of $H_r = -2.8$ kOe, where the resonance peak abruptly changes its sign, frequency, and slope, which indicates reversal of the vortex core polarity. Below the switching field $H < H_r$ the gyrotropic frequency of the inverted

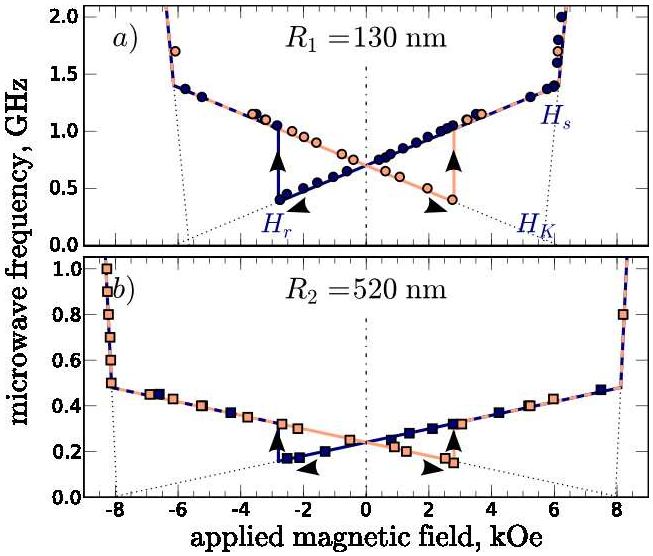

FIG. 2: (Color online) Frequency of the lowest excitation mode in a magnetic disk as a function of the perpendicular bias magnetic field for two sizes: (a) $R_1 = 130$ nm, (b) $R_2 = 520$ nm. Dark blue (light red) dots are experimental points corresponding to the field variation starting from large positive (negative) values. Solid lines are theoretical predictions from Eq. (1) for $|H| > H_s$ and from Eq. (2) for $|H| < H_s$.

vortex core increases like it did in positive bias fields before the core reversal. It is important to note, that upon *increasing* the bias field, the gyrotropic mode persists at reduced frequency until the symmetric reversal field of $H_r = +2.8$ kOe is reached, and the new reversal of the vortex core polarity takes place.

The complete phase diagrams demonstrating the dynamic hysteresis loops of the gyrotropic mode frequency in a perpendicular bias magnetic field for two disk sizes are presented in Fig.2. The dark blue dots correspond to the case when the bias field is reduced starting from large positive values, while the light red dots correspond to the opposite case, when the field is varied starting from large negative values.

Several important features emmerge in these phase diagrams: (i) For $|H| > H_s$ the excitation frequency of the lowest mode in the disk is well described by the Kittel's Eq. (1), and at $|H| = H_s$ the field slope of the mode frequency changes abruptly, while the expected discontinuity of the mode frequency is not seen in the experiment; (ii) In the interval $|H| < |H_r|$ each value of the bias field (except $H = 0$) corresponds to two different gyrotropic mode frequencies corresponding to two opposite orientations of the vortex core relative to the bias field, and the difference between these frequencies increases with the bias field H and with the disk aspect ratio β; (iii) The magnitude of the bias field $H = H_r$, at which the reversal of the vortex core polarity occurs, seems to be about the same for the two disks.

The frequency of the gyrotropic mode in the external perpendicular bias magnetic field H can be calculated as a ratio $\omega_G(H) = \kappa(H)/G(H)$ of the field-dependent vortex stiffness $\kappa(H)$ to the field-dependent magnitude $G(H)$ of the z-component of the vortex gyrovector using the method of Thiele's equation that was used in [6] to calculate this frequency in the case when $H = 0$. According to the general definition given in [6] (see Eq. (2) in [6]) when the perpendicular bias field is introduced we can write the vortex gyrovector as $G(H) = G(0)(1 - p\cos\theta)$, where $p = \pm 1$ is the vortex core polarity, $G(0)$ is the gyrovector in zero bias field defined in [6], and θ is the polar angle of the static magnetization at the disk lateral boundary. For a sufficiently large disk radius (much larger than the radius of the vortex core) is is possible to estimate θ from the standard electrodynamic boundary conditions at the vertical boundaries of the disk as $\cos\theta = H/H_s$.

The field-dependent vortex stiffness $\kappa(H)$ is found from the assumption that the main contribution to the vortex energy comes from the dipolar interaction of the volume magnetostatic charges created by the in-plane magnetization component of the shifted vortex outside the core [6]. In this region the in-plane magnetization components depend of the direction of the external bias field as $\sin\theta$, and the stiffness $\kappa(H)$, that is proportional to the square of the radial derivative of the in-plane magnetization, is expressed as $\kappa(H) = \kappa(0)\sin^2\theta$, where $\kappa(0)$ is the vortex stiffness in the zero bias field defined in [6]. Thus, we can write the explicit expression for the gyrotropic mode frequency in the perpendicular bias field as

$$\omega_G(H) = \omega_G(0)\left\{1 + p\frac{H}{H_s}\right\}, \qquad (2)$$

where $\omega_G(0)$ is the gyrotropic mode frequency in the zero bias field defined by Eq. (7) of [11]. The approximate expression for $\omega_G(0)$ obtained in the limit of small aspect ratios $\beta \ll 1$ has the form $\omega_G(0) = 5/(9\pi)4\pi\gamma M_s\beta$ [6]. The value of the saturation field H_s can also be determined as the crossing point of the dispersion curves (1) and (2). It occurs at $H_s \simeq H_K + 2\omega_G(0)/\gamma$ found to be ≈ 6.1 kOe for the smaller disk, a result that is close to the experimentally measured value shown in Fig.2a.

The theoretical curves calculated using Eq. (2) are shown by solid lines in Fig.2, and it is clear from this figure that Eq. (2) gives a good quantitative description of the experimental data for two different values of the disk aspect ratio. This simple analytic theory does not account for the reversal of the vortex core polarity observed experimentally at $H = H_r$ (see Fig.(2)). Therefore, we performed micromagnetic simulations to reproduce this experimentally observed effect. The results of these simulations are presented in Fig.3.

Our micromagnetic numerical code [12] calculates the stable configuration of the magnetization vector in the nano-disk by solving the Landau-Lifshitz (LL) equation

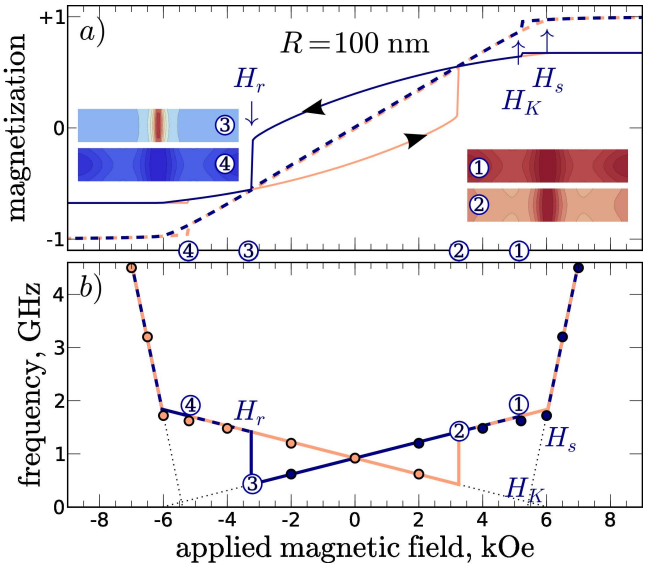

FIG. 3: (Color online)(a) Numerically calculated field dependence of the static magnetization of the NiMnSb disk (thickness $t = 43.75$ nm, radius $R = 100$ nm): the hysteretic behavior of the static magnetization, M_z, averaged over the disk volume (dashed loop) and over the vortex core (solid loop). The inserts show the spatial distribution of M_z at four progressively decreasing values of H. (b) Resonance locus calculated by the 3D micromagnetic code (dots) along with the analytical model (solid lines).

in the time domain. A 3D mesh with a cubic cell of size 3.125 nm gives a discrete representation of the nano-disk magnetization. The nano-disk dimensions were chosen as $R = 100$ nm, $t = 43.75$ nm, while the values of the magnetic parameters were taken from table I. The numerically calculated static hysteresis loop of $M_z(H)$ (where the vertical component of the static magnetization M_z was averaged over the disk volume) is shown in Fig.3a by a dashed line. Color images of M_z distribution across the radial section of the disk taken at four points corresponding to progressively decreasing values of the perpendicular bias magnetic field H are shown as inserts in Fig.3a. Although the vortex core switching is not seen in this *averaged* static hysteresis loop, it is clearly revealed when the averaging of the static M_z component is done over the spatial region occupied by the vortex core ($\simeq 15$ nm), as demonstrated by the solid lines in Fig.3a, where the core polarity switching appears as a jump at $|H_r| = 3.25$ kOe.

The *dynamic* hysteresis loop (i.e. the dependence of the gyrotropic mode frequency on the perpendicular bias magnetic field H) shown in Fig.3b was numerically calculated using a second code developed by the authors, which computes the full dynamic susceptibility tensor χ'' from linearization of the LL equation around the equilibrium configuration [12]. It clearly demonstrates the effects of the bias-field-induced dynamic bistability [13] in the field interval $|H| < H_r$, and the gyrotropic frequency jumps at $H = \pm H_r$, associated with the reversal of the vortex core polarity taking place at the same bias field values (see Fig.3a). Numerical simulations performed for a nano-disk of radius $R' = 250$ nm gave results that are qualitatively similar to the one shown in Fig.3 for $R = 100$ nm, but the vortex core reversal field was found to be $|H_r'| = 2.75$ kOe. Qualitatively, the polar angle of the curled magnetization at the periphery, θ, which stabilizes the vortex in the opposite orientation and favors the existence of the bistablity phase, decreases with increasing aspect ratio. Experimentally, the vortex core reversal field for both experimentally measured nano-disks ($R_1 = 130$ and $R_2 = 520$ nm) was close $|H_r| = 2.8$ kOe. We believe that the main reason for this is the influence of the stray field of the MRFM probe (Fe sphere) which was stronger for the smaller nano-disk and accounts well for the observed discrepancy of about 500 Oe with the numerical simulations.

This research was partially supported by the ANR PNANO06-0235 from France, by the European Grant DynaMax (FP6-IST 033749), by the MURI Grant No. W911NF-04-1-0247 from the U.S. Army Research Office, by the Contract W56HZV-08-P-L605 from the U.S. Army TARDEC, RDECOM, and by the Grant No. ECCS-0653901 from the U.S. National Science Foundation. K.G. acknowledges support by the Ikerbasque Science Foundation.

* Corresponding author; Electronic address: gregoire.deloubens@cea.fr

[1] R. P. Cowburn, D. K. Koltsov, A. O. Adeyeye, M. E. Welland, and D. M. Tricker, Phys. Rev. Lett. **83**, 1042 (1999).
[2] T. Shinjo, T. Okuno, R. Hassdorf, K. Shigeto, and T. Ono, Science **289**, 930 (2000).
[3] B. V. Waeyenberge, A. Puzic, H. Stoll, K. W. Chou, T. Tyliszczak, R. Hertel, M. Fähnle, H. Brückl, K. Rott, G. Reiss, et al., Nature (London) **444**, 461 (2006).
[4] M. Curcic, B. V. Waeyenberge, A. Vansteenkiste, M. Weigand, V. Sackmann, H. Stoll, M. Fähnle, T. Tyliszczak, G. Woltersdorf, C. H. Back, et al., Phys. Rev. Lett. **101**, 197204 (2008).
[5] K. Yamada, S. Kasai, Y. Nakatani, K. Kobayashi, H. Kohno, A. Thiaville, and T. Ono, Nature Mater. **6**, 270 (2007).
[6] K. Guslienko, B. Ivanov, V. Novosad, Y. Otani, H. Shima, and K. Fukamichi, J. Appl. Phys. **91**, 8037 (2002).
[7] O. Klein, G. de Loubens, V. V. Naletov, F. Boust, T. Guillet, H. Hurdequint, A. Leksikov, A. N. Slavin, V. S. Tiberkevich, and N. Vukadinovic, Phys. Rev. B **78**, 144410 (2008).
[8] P. Bach, A. S. Bader, C. Rüster, C. Gould, C. R. Becker, G. Schmidt, L. W. Molenkamp, W. Weigand, C. Kumpf, E. Umbach, et al., Appl. Phys. Lett. **83**, 521 (2003).

[9] G. N. Kakazei, P. E. Wigen, K. Y. Guslienko, V. Novosad, A. N. Slavin, V. O. Golub, N. A. Lesnik, and Y. Otani, Appl. Phys. Lett. **85**, 443 (2004).
[10] V. Novosad, F. Y. Fradin, P. E. Roy, K. S. Buchanan, K. Y. Guslienko, and S. D. Bader, Phys. Rev. B **72**, 024455 (2005).
[11] K. Y. Guslienko, J. Nanosci. Nanotechnol. **70**, 2745 (2008).
[12] F. Boust and N. Vukadinovic, Phys. Rev. B **70**, 172408 (2004).
[13] F. Giesen, J. Podbielski, T. Korn, M. Steiner, A. van Staa, and D. Grundler, Appl. Phys. Lett. **86**, 112510 (2005).